Solid Earth Discuss., 6, 559–598, 2014
www.solid-earth-discuss.net/6/559/2014/
doi:10.5194/sed-6-559-2014

Solid Earth Discussions
Open Access

A new model of the upper mantle structure beneath the western rim of the East European Craton

M. Dec[1], M. Malinowski[1], and E. Perchuc[2]

[1]Institute of Geophysics, Polish Academy of Sciences, Ks. Janusza 64, 01-452 Warsaw, Poland
[2]Bernardynska 21/57, 02-904 Warsaw, Poland

Received: 27 January 2014 – Accepted: 30 January 2014 – Published: 14 February 2014

Correspondence to: M. Dec (monikadec@igf.edu.pl) and E. Perchuc (perchuc.ed.geo@gmail.com)

Published by Copernicus Publications on behalf of the European Geosciences Union.

Abstract

In this article we present a new 1-D *P* wave seismic velocity model (called MP1-SUW) of the upper mantle structure beneath the western rim of the East European Craton (EEC) based on the analysis of the earthquakes recorded at the Suwałki (SUW) seismic station located in NE Poland which belongs to the Polish Seismological Network (PLSN). This analysis was carried out due to the fact that in the wavefield recorded at this station we observed a group of reflected waves after expected $P_{410}P$ at epicentral distances 2300–2800 km from SUW station. Although the existing global models represent the first arrivals, they do not represent the full wavefield with all reflected waves because they do not take into account the structural features occurring regionally such as 300 km discontinuity. We perform *P* wave traveltime analysis using 1-D forward ray-tracing modelling for the distances up to 3000 km. We analysed 249 natural seismic events that were divided into four azimuthal spans with epicentres in the western Mediterranean Sea region (WMSR), the Greece and Turkey region (GTR), the Caucasus region (CR) and the part of the North Atlantic Ridge near the January Mayen Island (JMR). Events from each group were sorted into four seismic sections respectively. The MP1-SUW model documents bottom of the asthenospheric low velocity zone (LVZ) at the depth of 220 km, 335 km discontinuity and the zone with the reduction of *P* wave velocity atop 410 km discontinuity which is depressed to 440 km depth. The nature of a regionally occurring 300 km boundary here we explained by tracing the ancient subduction regime related to the closure of the Iapetus Ocean, the Rheic Ocean and the Tornquist Sea.

1 Introduction

One-dimensional reference models are employed almost in every seismological method aimed at imaging the Earth's interior (tomography, receiver functions, underside reflections). However, results of those methods can be biased by the choice of the

SED
6, 559–598, 2014

background velocity model (e.g. Bastow, 2012). Therefore, in the regional studies, it might be more appropriate to use modified reference models taking into account, e.g. the tectonic regime of the area (e.g. Thybo and Perchuc, 1996). Following this strategy, we attempt to derive a one-dimensional upper mantle *P* wave velocity model for the areas surrounding the East European Craton (EEC) to the west and to the south. Toward this end, we use the data recorded at the Suwałki (SUW) station belonging to the Polish Seismological Network. The data registered at the SUW station has been the object of much scientific interest (e.g. Bock et al., 1997, Świeczak et al., 2004; Wilde-Piórko, 2005), but none of these were focusing on the detailed interpretation of the recorded traveltimes in the far-regional mode.

Due to the advancement in instrumentation and access to infrastructure, array seismology is developing rapidly (e.g. the Earthscope, USArray project, Levander, 2003). However, the cost of experiments remain very high. Here we would like to explore the concept of using single-station data from the existing seismological network to study the upper mantle structure based on traveltimes and amplitudes of the body waves. The necessary prerequisite for performing such a study is the selection of the station that is located optimally for imaging particular mantle structure by providing proper azimuthal span and epicentral distances of the recorded earthquakes (see e.g. Nita et al., 2012).

The choice of the SUW station for this analysis is twofold. First of all, it is characterized by a good signal-to-noise ratio and relatively simple wavefield, as it is located on the stable part of the EEC with a thin sedimentary cover. Secondly, the earthquakes recorded from 4 azimuthal sectors (North Atlantic Ridge, Western Mediterean Sea, Greece-Turkey, Caucasus) are located in the 1500–3000 km epicentral distance range, providing proper illumination of the upper mantle structure between the base of the asthenosphere and the 410 km discontinuity. The bottoming points of the refracted waves and midpoints of the reflected waves fall in to the south-western rim of the East European Craton as indicated in Fig. 1. Therefore, we can study the influence of the Teisseyre-Tornquist Zone (TTZ) on the recorded wavefield and mantle structure.

SED
6, 559–598, 2014

First we present tectonic setting and a review of the studies pertaining to the investigated area, which mainly focused on the Earth's crust. Subsequently, we describe data (seismic waveforms from natural seismic events) and method used in this analysis (1-D and 2-D ray-tracing modelling). In the results section we present all analysed seismic sections together with the traveltimes calculated for our preferred upper mantle model. It is followed by a brief analysis of the errors and traveltime residuals statistics. Finally, we discuss our results in the context of the geodynamics of the circum-EEC region.

2 Tectonic setting and previous geophysical investigations

In order to understand the structure and nature of the upper mantle below the Baltica, it is necessary to understand its history as a paleocontinent which was moving across Iapetus Ocean with other paleocontinets and microplates which nowadays are in direct contact with Baltica. The EEC is the oldest part of Eastern Europe. It formed about 1.8–1.7 Ga yr ago as a result of a collision between three separate plates: Fenoscandia, Sarmatia and Volgo-Uralia (Bogdanova et al., 2001; Bogdanova, 2005). The history of paleoplate movements from Vendian to Permian was described by Cocks and Torsvik (2006). There were two major paleotectonical events. First, about 450 Ma in the Ordovician, Avalonia separated from Gondwana and docked with Baltica and afterwards they both joined to Laurentia. The last event was connected with the closure of the Iapetus Ocean which ended about 420 Ma and the closure of the Tornquist Sea – a branch of Iapetus. A different situation had place in the SW part of the cratonic rim. In this area there were Rheic Ocean structures formed from Devonian to Permian and then the Paleothetydian, which were evolving up to the TTZ (Ziegler and Dèzes, 2006). On the whole structures from the NW and SW part of the EEC there were imposed Caledonian structures, Northwest Highlands (Gee, 1975) and Polish Caledonides (Znosko, 1986).

Geophysical research is mainly seismic. There were numerous deep seismic sounding profiles recorded both west and east of the TTZ (Guterch et al., 2010). Starting with the LT profiles located in Poland (Guterch et al., 1986), through the EUGENO-S in Den-

SED
6, 559–598, 2014

mark and southern Sweden (EUGENO-S Working Group et al., 1988), Polish projects POLONAISE'97 (Guterch et al., 1999) and CELEBRATION 2000 (Guterch et al., 2001), FENNOLORA transect (Guggisberg and Berthelsen, 1987; Abramovitz et al., 2002), BABEL project (BABEL Working Group, 1991), MONA LISA (Abramovitz et al., 1998) or EUROBRIDGE (EUROBRIDGE Seismic Working Group, 1999) we achieved information about crustal structure of the EEC and surrounding areas.

All these projects provided gross crustal structure down to the Moho and only in a few cases deeper boundaries were interpreted (Grad et al., 2002). During the acquisition of the deep seismic sounding profiles, some upper mantle phases (both reflections and refractions) were traced in the offset range beyond 400 km (e.g. in project POLONAISE'97, Grad et al., 2002; EUGENO-S Working Group, 1988; BABEL Working Group, 1993; MONA LISA, Abramovitz et al., 1998). Apart from the controlled-source seismology, some passive-source experiments were conducted with the TOR project being the most significant (Gregersen et al., 2010; Plomerová et al., 2002). The TOR project spanning about 1000 km from northern Germany, through Denmark up to southern Sweden, crossed principal tectonic zones inside the rim of the EEC such as the Variscan Front, the Caledonian Deformation Front and the Sorgenfrei–Tornquist Zone – the northern extension of the TTZ. This allowed to image seismic structure of the crust and the upper mantle (e.g. Somali et al., 2006; Gregersen et al., 2010). Recently conducted PASSEQ project (Wilde-Piórko et al., 2008) provided the data for the analysis of *P* wave receiver function beneath the western edge of the EEC and adjacent Phanerozoic Europe across the TTZ (Knapmeyer-Endrun et al., 2013).

3 Data and method

The Suwałki (SUW) seismic station was chosen for this study because of the good recording conditions in the remote part of NE Poland and thin sediment cover resulting in high-quality seismic signal registrations. The station is equipped with the STS-2 sensor and the data were sampled at 20 Hz. We used broad-band data recorded between

SED
6, 559–598, 2014

1997–2010 for earthquakes with magnitude greater than 4.5. The hypocenter locations were taken from the ISC bulletin (http://www.isc.ac.uk/iscbulletin). The retrieved waveforms were converted from the native MSEED to SEG-Y format in order to make seismic record sections suitable for interpretation and modelling using standard tools used in controlled-source seismology (Zelt, 1994).

The analysed 249 events (see Appendix 1 and Fig. 1) had epicenters located in the following areas:

1. rift zone around the Jan Mayen region in the northern Atlantic (JMR),
2. Western Mediterranean Sea region (WMSR),
3. Greece and Turkey region (GTR),
4. Caucasus region (CR).

All earthquakes generated in the JMR (part of the Mid-Atlantic Ridge) (Fig. 2a) were shallow crustal ones (depth down to 10 km). The focal depths in the WMSR were also shallow, down to 20 km (Fig. 2b). However, the data from the GTR (Fig. 2c) and CR (Fig. 2d), due to a large variability of the source depths, were separated into three groups with the focal depth ranges: 0–20 km, 20–50 km and > 50 km.

We divided earthquakes into these ranges of depth after observation of changes in AK135 model calculated for different focal depths. We evaluated differences in travel-times by calculating them for different focal depths. It allowed us to separate events into smaller groups. Modelling was performed for each group separately. It allowed us to limit static shifts in the record sections to 1 s. In a case of diversified focal depth ranges between the events referring to the same epicentral group, we did not apply focal depth corrections while bringing the data together in a seismic section.

Seismic record sections sorted according to the increasing epicentral distance consist of the following number of seismograms: 34 (JMR), 43 (WMR), 103 (GTR), 69 (CR). We tested a range of band pass filter frequencies for displaying data and finally concluded that the best results were obtained for 0.5–2.0 Hz bandwidth. As a check of

SED
6, 559–598, 2014

data quality we calculated signal-to-noise (SNR) ratio, estimated using energy of the signal in the 2 s wide window before and after first arrivals. Calculations were made in the ZPLOT software (Zelt, 1994). Table 2 shows mean SNRs calculated for the individual group of events. Group of the deepest earthquakes from the GTR are characterised by the best SNR for raw data. The best improvement after filtering was observed for the CR group for events with focal depth range 0–20 km. The average SNR for all raw data is 5.38 and after filtering 0.5–2.0 Hz we achieve improvement of ∼ 68 %.

The observed reflectivity can be aligned based on the maximum amplitude (Fig. 3). Good alignment was obtained for the phase emerging at the time of the 410 km discontinuity (Fig. 3a). There are also some other strong events that can be aligned in the epicentral distance of 2260–2430 km (Fig. 3b), later interpreted as being the reflection event from around 300 km depth. Other reflected and refracted upper mantle arrivals can be distinguished in the record sections (Figs. 4–7). The following seismic phases were interpreted during subsequent modelling: P_{220} – refracted wave from the bottom of the asthenosphere (LVZ), $P_{335}P$ – reflected wave from regionally occurring discontinuity located at the depth of about 335 km, and P_{440} and $P_{440}P$ – refracted and reflected waves from 440 km discontinuity.

We used forward trial-and-error one-dimensional (Kamiński and Müller, 1979) or two-dimensional ray-tracing modelling (Gorman, 2002) in order to fit the observed travel-times of the refracted and reflected *P* wave mantle phases and derive upper mantle

P wave velocity models beneath the areas indicated in Fig. 1b. Finally, models were verified by calculating synthetic seismograms using the reflectivity method (Fuchs and Müller, 1971; Müller, 1985).

4 Results

We begin our modelling with the analysis of the MP-1 model derived for the seismically active part of the United States (Perchuc et al., 2008), west of the North American Cra-

SED
6, 559–598, 2014

ton. The North American Craton was created in the same time as the EEC (Hoffman, 1988) and is characterized by similar features, which justifies such an analysis.

Figure 4a shows the obtained velocity distribution beneath the western rim of the EEC (MP1-SUW model, Table 3) resulting from the forward ray-tracing modelling and fitting of the calculated traveltimes to the observed mantle arrivals (Figs. 4–7). Because of the far-offset range used in this study, the velocities in the crust and down to 8° degree discontinuity (ca. 100 km depth, Thybo and Perchuc, 1997) were introduced a priori and fixed during modelling. Crustal part of the models was based on the published deep seismic sounding results (e.g. Guterch et al., 1986; Grad et al., 2009).

In case of the JMR group, the waves leaving the source propagated within the oceanic crust first and then went through the continental-type lithosphere. Therefore, 2-D modelling was necessary to account for the variability between the oceanic and continental lithosphere encountered along this transect (Fig. 7b). The continental part has similar vertical distribution of velocity to 1-D models for other azimuths.

Figure 4 shows the seismic sections for the area of Greece and Turkey. Most of the events in this region occur down to 20 km depth and the epicentral distances for those events are from 1500 to 2300 km (Fig. 4b). There is a good fit between the data and the traveltimes refracted at the base of the mantle LVZ (red dashed line) at the depth of 220 km. It is observed in the first arrivals up to 2100 km. The $P_{335}P$ (blue line) occurs as secondary arrivals. At an epicentral distance of about 2100 km, there is an intersection of the traveltime branches of P_{220} and P_{440} (green dashed line) phases. After 2100 km offset branch of P_{440}(green dashed line) is observed in first arrivals.

Figure 4c shows the earthquakes from the focal depth range of 20–50 km. These events were recorded at epicentral distances ranging from 1500 to 2300 km. As in the previous group, the P_{220} phase is observed in first arrivals at distances up to about 2100 km. After 2100 km the P_{440} phase arrives first. The $P_{335}P$ wave is also visible as a second group. $P_{440}P$ is also recorded in the form of high amplitude signals observed at distances from 1950 to 2300 km. The closer the distance of 2250 km, the more diffi-

SED
6, 559–598, 2014

cult it is to separate $P_{335}P$ and $P_{440}P$ because these two branches intersect each other at this point.

Figure 4d shows the deepest group of earthquakes (focal depth > 50 km) recorded at the epicentral distances of 1860 to 2140 km. P_{220} can be seen only on two seismograms. Although, its presence at this depth is documented in the previous two sections. On this section the $P_{335}P$ and $P_{440}P$ reflected phases are also observed.

Figure 5 show the seismic sections for the Caucasus region. Records from these events start at about 2000 and end at about 3000 km epicentral distance. Here we also divided data into three focal depth ranges: 0–20 km depth (Fig. 5a), 20–50 km depth (Fig. 5b) and > 50 km (Fig. 5c). In this case, we can only observe first arrivals in the first two sections of P_{220} (red dashed line). However, analysing the wavefield allows us to follow phases refracted from 440 km and reflected from 335 and 440 km. On each section we have records documenting intersection of the two branches: $P_{335}P$ and $P_{440}P$ at 2250 km, after which in the second arrivals we observed $P_{440}P$ and next $P_{335}P$.

In case of the Western Mediterranean group of events, there is almost the whole range of observed epicentral distances. The shallow focal depth range, 0–20 km, allows us to put all events together in one seismic section (Fig. 6). Here we can observe P_{200} in its first arrivals at distances from 1700 to 2000 km. At these distances we observe high-amplitude $P_{335}P$ and $P_{440}P$ as secondary arrivals. There is a lack of seismograms in the area, where traveltime branches of P_{200} and P_{440} intersect, but after 2200 km we observe P_{440} in its first arrivals. Next we observed $P_{440}P$ and then $P_{335}P$ phase.

Figure 7a presents the seismic section for the Jan Mayen region. All those earthquakes are located along the rift zone close to the Jan Mayen Island region in the northern Atlantic. Their focal depths are from 0 to 10 km. The recorded epicentral distances ranging from 2260 to 2720 km allow us to model 335 km and 440 km discontinuities. Taking into account differences in the oceanic and continental lithosphere, we build a 2-D velocity model. We observe P_{440} in its first arrivals and $P_{440}P$ in the second.

SED
6, 559–598, 2014

The $P_{335}P$ is also observed in this seismic section. Figure 7b illustrates waves propagation, reflections at 335 km and refractions and reflections at 440 km discontinuities.

Figure 8 presents all 249 earthquakes with focal-depth traveltime corrections applied on one seismic section. We added values consequent from different focal depth for each group respectively. These values were calculated during separation of earthquakes into smaller groups. In order to verify the credibility of the derived models, we calculated synthetic seismograms using reflectivity method (Fuchs and Müller, 1971; Müller, 1985). There is a good amplitude match between the recorded data (Fig. 8) and the synthetic section (Fig. 9).

There is an interesting feature in the MP1-SUW model presented here (Fig. 4a). Atop the 440 km discontinuity there is a 10 km thick zone with reduced velocities. The insertion of the LVZ is necessary to explain the separation between P_{440} and $P_{440}P$ branches as shown in Fig. 10. Figure 10a contains part of a section from Fig. 8 with the traveltimes calculated for the MP1-SUW model and Fig. 10b shows the same section with the traveltimes calculated for the model without the LVZ but with the same average velocity preserved.

5 Error analysis

We picked all the phases with the accuracy of ±0.1 s. The most significant uncertainties are attributed to the limited accuracy of the event location. The focal depth is the most uncertain hypocentre coordinate in the ISC bulletins, which were used in this analysis.

In order to demonstrate how well the predicted traveltimes are fitted to the observed data, we present histograms of traveltime residuals (Tobs. – Tres.) in Fig. 11. We compare the traveltime residuals of the first arrivals calculated for the MP1-SUW model (Fig. 11a–e) and for the reference AK135 model (Kennett et al., 1995) (Fig. 11a'–e').

Figure 11a and 11a' show histograms for all used earthquakes. The adjustment for our model is better than for the AK135. There are smaller errors for −0.5–0.5 s range. The best fit was obtained for the Jan Mayen group of events (Fig. 11d). The traveltime

SED
6, 559–598, 2014

residual range for that region is ±1 s. We attribute such a good fit to small focal depth uncertainties of the earthquakes from that region. Events with small focal differences are more unique. It could also be a result of the two-dimensional modelling.

The MP1-SUW model predicts two new branches of traveltimes for reflected waves, the $P_{335}P$ and $P_{440}P$. Figure 12 presents how they fit in the records collected at the SUW station. In case of other models, such as PREM (Dziewoński, 1981), IASPEI91 (Kennett and Engdahl, 1991), AK135 (Kennett et al., 1995) or iPREF (Cammarano and Romanowicz, 2008) there is no possibility to make such analysis because they do not reflect regional-scale inhomogeneities.

In Table 4 we summarized the three parameters of the fitting quality: the standard deviation, variance, kurtosis and root mean square for all groups of data. Kurtosis is a measure of the deviation from the normal distribution (the kurtosis of the normal distribution is 3 for the applied formula). Distributions that have higher variation than the normal distribution have kurtosis greater than 3, distributions with lower variation have kurtosis less than 3.

Presented summary of the traveltime residuals' statistics shows the fitting parameters with respect to the MP1-SUW model and the AK135 respectively. We subdivided GTR and CR analysis into smaller groups according to focal depths respectively. The calculated results are also the best for the JMR. The comparison of the data in Table 2 shows that the experimental data is described better by our model than the global reference AK135. Although AK135 model describes first arrivals well, it does not take into account reflected waves and regional discontinuities such as 300 km discontinuity.

6 Discussion

The MP1-SUW model is intended to characterise the western rim of the EEC. Both 1-D and 2-D models give a consistent image of the upper mantle structure beneath the western rim of the EEC. The Lehmann 220 km phase, defining the bottom of the low velocity zone (Lehmann, 1961), is seen in first impulses for the distance range

SED
6, 559–598, 2014

1500–2150 km. A very prominent feature of the MP1-SUW model is the existence of the 300 km discontinuity at the depth of 335 km, which is observed at 1500–2800 km offset range. The origin of the 300 km discontinuity is generally related to the existence of a subduction zone (Revenaugh and Jordan, 1991), where increased amount of free silica is delivered to the upper mantle by subducted oceanic and continental material. Both coesite–stishovite phase transformation and thermal anomaly provided by subducting slab can explain the velocity jump at this discontinuity (Liu et al., 1999). With relation to the Mechanical Mixture model by Xu et al. (2008), jump in *P* wave velocity around 335 km depth would require enrichment in the basaltic component. In this region, the nature of this boundary can be tentatively explained as the traces of the ancient subduction regime related to the closure of the Iapetus and Rheic Oceans and the Tornquist Sea (e.g. Torsvik and Rehnström, 2003). This discontinuity, due to its regional-scale, is recorded better for JMR and CR groups of events, although we observe it also for WMSR and GTR groups. An independent support for the existence of such a discontinuity was recently provided by Knapmeyer-Endrun et al. (2013) who studied *P* wave receiver function based on the data from the PASSEQ experiment. There is a clear peak observed in the receiver function section clustered around TTZ at ca. 30 s relative time (see Fig. 7 in Knapmeyer-Endrun et al., 2013), which is roughly equivalent to ca. 300 km depth. Although, authors do not comment whether this signal is related to primary or multiple energy.

We modelled 410 km discontinuity at the depth of 440 km. It is observed in first impulses at the offset range of 2150–3100 km. The deeper location of the discontinuity compared to the reference global model (e.g. AK135) relates to the observation of the LVZ atop it. We find reports of such a zone in regional-scale investigations (Thybo et al., 1997). It was also postulated as the global phenomenon (Bercovici and Karato, 2003). In this case it can also be explained as an ancient oceanic structure subducted during the closure of the Tornquist Sea (Torsvik and Rehnström, 2003). The low-velocity zone above 410 km discontinuity we interpret as a result of the dehydration of the subducted plate that brought some residual water in the transition zone.

SED
6, 559–598, 2014

This feature was found and documented also in the western part of the United States (Song et al., 2004), where authors interpreted it as a compositional anomaly. It could be caused by a dense partially-melted layer linked to prior subduction of the Farallon plate and back-arc extension.

7 Conclusions

We derived a new *P* wave velocity model of the upper mantle structure characterising the western rim of the East European Craton (model MP1-SUW). Analysing seismic record sections from events recorded at the SUW station, we calculated one-dimensional *P* wave velocity model for the azimuthally-differentiated regions: the Western Mediterranean Sea region, the Greece and Turkey region and the Caucasus region. Two-dimensional model for the JMR region was justified by the fact that waves propagating from that source region go through the oceanic and continental structures.

The MP1-SUW model documents bottom of the asthenospheric low velocity zone at the depth of 220 km, 335 km discontinuity and the zone with the reduction of *P* wave velocity atop 410 km discontinuity which is depressed to 440 km depth. The nature of both the 335 km and 440 km discontinuities are explained by tracing the ancient subduction regime related to the closure of the Iapetus and Rheic Oceans and the Tornquist Sea (Torsvik and Rehnström, 2003). The 335 km discontinuity is a robust feature of the MP1-SUW model, however we are aware that this feature is not ubiquitous, but linked to the marginal zone of the EEC.

The work presented here shows that even a single station can be a rich source of information when a careful phase identification and modelling are implemented. We hope that the seismological community will benefit from the use of the MP1-SUW model in other regional studies, e.g. receiver function calculation or traveltime tomography.

SED
6, 559–598, 2014

The Supplement related to this article is available online at doi:10.5194/sed-6-559-2014-supplement.

Acknowledgements. This study has been funded by National Science Centre. Grant No. DEC-2011/01/N/ST10/07275. We are very grateful to Dr. Piotr Środa for fruitful discussions. Some of the figures were prepared using Generic Mapping Tool software (Wessel and Smith, 1995).

References

Abramovitz, T., Thybo, H., and MONA LISA Working Group: Seismic structure across the Caledonian deformation front along MONA LISA profile 1 in the southeastern North Sea, Tectonophys, 288, 153–176, 1998.

Abramovitz, T., Landes, M., Thybo, H., Jacob, A. W. B., and Prodehl, C.: Crustal velocity structure across the Tornquist and Iapetus Suture Zones – a comparison based on MONA LISA and VARNET data, Tectonophys, 314, 69–82, 1999.

Abramovitz, T., Thybo, H., and Perchuc, E.: Tomographic inversion of seismic *P* and *S* wave velocities from the Baltic Shield based on FENNOLORA data, Tectonophys, 358, 151–174, 2002.

BABEL Working Group: Evidence for early Proterozoic plate tectonics from seismic reflection profiles in the Baltic Shield, Nature, 348, 34–38, 1991.

BABEL Working Group: Deep seismic reflection/refraction interpretation of crustal structure along BABEL profiles A and B in the southern Baltic Sea, Geophys. J. Int., 112, 325–343, 1993.

Bastow, I. D.: Relative arrival-time upper-mantle tomography and the elusive background mean, Geophys. J. Int., 190, 1271–1278, 2012.

Bercovici, D. and Karato, S.: Whole-mantle convection and the transition-zone water filter, Nature, 425, 39–44, 2003.

Bock, G., Perchuc, E., Hanka, W., Wiejacz, P., Kind, R., Suchcicki, J., and Wylengalla, K.: Seismic anisotropy beneath the Suwalki station: one year of the activity of the station, Acta Geophys. Pol., 45, 1–12, 1997.

Bogdanova, S. V., Gorbatschev, R., and Stephenson, R. A.: EUROBRIDGE: paleoproterozoic accretion of Fennoscandia and Sarmatia, Tectonophys, 339, vii-x, 2001.

SED
6, 559–598, 2014

Bogdanova, S. V., Gorbatschev, R., and Garetsky, R. G.: The East European craton, in: Encyclopedia of Geology, edited by: Selley, R. C., Cocks, L. R., and Plimer, I. R., Elsevier, 2, 34–49, 2005.
Cammarano, F. and Romanowicz, B.: Radial profiles of seismic attenuation in the upper mantle based on physical models, Geophys. J. Int., 175, 116–134, 2008.
Cocks, L. R. M. and Torsvik, T. H.: European geography in a global context from the Vendian to the end of the Palaeozoic, in: European Lithosphere Dynamics, edited by: Gee, D. G. and Stephenson, R. A., Geological Society, London, Memoirs, 32, 83–95, 2006.
Dziewoński, A. and Anderson, D.: Preliminary reference Earth model, Phys. Earth Planet. In., 25, 297–356, 1981.
EUGENO-S Working Group: Crustal structure and tectonic evolution of the transition between the Baltic Shield and the North German Caledonides (the EUGENO-S Project), Tectonophys, 150, 253–348, 1988.
EUROBRIDGE Seismic Working Group: Seismic velocity structure across the Fennoscandia-Sarmatia suture of the East European craton beneath the EUROBRIDGE profile through Lithuania and Belarus, Tectonophys, 314, 193–217, 1999.
Fuchs, K. and Müller, G.: Computation of synthetic seismograms with the reflectivity method and comparison with observations, Geophys. J. Roy. Astr. S., 23, 417–433, 1971.
Gee, D. G.: Tectonic model for central part of scandinavian caledonides, Am. J. of Sci., A275, 468–515, 1975.
Gorman, A. R.: Ray-theoretical seismic traveltime inversion – modifications for a two-dimensional radially parametrized Earth, Geophys. J. Int., 151, 511–516, 2002.
Grad, M., Keller, G. R., Thybo, H., Guterch, A., and POLONAISE Working Group: Lower lithospheric structure beneath the Trans-European Suture Zone from POLONAISE'97 seismic profiles, Tectonophys, 360, 153–168, 2002.
Grad, M., Tiira, T., and ESC Working Group: The Moho depth map of the European Plate, Geophys. J. Int., 176, 279–292, 2009.
Gregersen, S., Voss, P., Nielsen, L. V., Achauer, U., Busche, H., Rabbel, W., and Shomali, Z. H.: Uniqueness of modeling results from teleseismic *P* wave tomography in Project Tor, Tectonophys, 481, 99–107, 2010.
Guggisberg, B. and Berthelsen, A.: A two-dimensional velocity model for the lithosphere beneath the Baltic Scield and its possible tectonic significance, Terra Cognita, 7, 631–638, 1987.

SED
6, 559–598, 2014

Guterch, A., Grad, M., Materzok, R., Perchuc, E., and Toporkiewicz, S.: Results of seismic crustal studies in Poland, Publ. Inst. Geophys. Pol. Acad. Sci., 17, 84–89, 1986.
Guterch, A., Grad, M., Materzok, R., and Perchuc, E.: Deep structure of the Earth's crust in the contact zone of the Paleozoic and Precambrian Platforms in Poland (Tornquist-Teisseyre zone), Tectonophys, 128, 251–279, 1996.
Guterch, A., Grad, M., Thybo, H., Keller, G. R., and POLONAISE Working Group: POLONAISE'97 – international seismic experiment between Precambrian and Variscan Europe in Poland, Tectonophys, 314, 101–121, 1999.
Guterch, A., Grad, M., and Keller, G. R.: Seismologists celebrate the new Millennium with an experiment in Central Europe, EOS Trans. AGU, 82, 529, 534–535, 2001.
Guterch, A., Wybraniec, S., Grad, M., Chadwick, R. A., Krawczyk, C. M., Ziegler, P. A., Thybo, H., and Vos, W. D.: Crustal structure and structural framework, in: Petroleum Geological Atlas of the Southern Permian Basin Area, edited by: Doornenbal, J. C. and Stevenson, A. G., EAGE Publications B. V., 11–23, 2010.
Hoffman, P. F.: United Plates of America, the birth of a craton: early proterozoic assembly and growth of Laurentia, Annu. Rev. Earth Pl. Sc., 16, 543–603, 1988.
ISC Bulletin, available at: http://www.isc.ac.uk/iscbulletin (last access: May 2013), 2013.
Kamiński, W. and Müller, G.: Program LAUFZEIT, University of Karlsruhe, 1979.
Kennett, B. L. N. and Engdahl, E. R.: Travel times for global earthquake location and phase identification, Geophys. J. Int., 105, 429–465, 1991.
Kennett, B. L. N., Engdahl, E. R., and Buland, R.: Constraints on seismic velocities in the earth from travel times, Geophys. J. Int, 122, 108–124, 1995.
Knapmeyer-Endrun, B., Krüger, F., Legendre, C., Geissler, W., and PASSEQ Working Group: Tracing the influence of the Trans-European Suture Zone into the mantle transition zone, Earth Planet. Sc. Lett., Elsevier, 363, 73–87, 2013.
Liu, J., Zhang, J., Flesch, L., Li, B., Weidner, D., and Liebermann, R.: Thermal equation of state of stishovite, Phys. Earth Planet. In., 112, 257–266, 1999.
Lehmann, I.: S and the Structure of the Upper Mantle, Geophys. J. Roy. Astr. S., 4, 124–138, 1961.
Levander, A.: USArray design implications for wavefield imaging in the lithosphere and upper mantle, The Leading Edge, 22, 250–255, 2003.
Müller, G.: The reflectivity method: a tutorial, J. Geophys., 58, 153–174, 1985.

SED
6, 559–598, 2014

Nita, B., Dobrzhinetskaya, L., Maguire, P., and Perchuc, E.: Age-differentiated subduction regime: An explanation of regional scale upper mantle differences beneath the Alps and the Variscides of Central Europe, Phys. Earth Planet. In., 206–207, 1–1, 2012.
Perchuc, E. and Thybo, H.: A new model of upper mantle *P* waves velocity below the Baltic Shield, Indication of partial melt in the 95 to 160 km depth range, Tectonophys, 253, 227–245, 1996.
Perchuc, E., Malinowski, M., and Nita, B.: Seismic and petrological properties of the upper mantle between 300 and 400 km depth, AGU Fall Meeting, S14C-01, 2008.
Plomerová, J., Babuška, V., Vecsey, L., and Kouba, D.: Seismic anisotropy of the lithosphere around the Trans-European Suture Zone (TESZ) based on teleseismic body-wave data of the TOR experiment, Tectonophys, 360, 89–114, 2002.
Revenaugh, J. and Jordan, T.: Mantle layering from ScS reverberations: the upper mantle, J. Geophys. Res., 96, 19781–19810, 1991.
Shapiro, N. M. and Ritzwoller, M. H.: Monte-Carlo inversion for a global shear velocity model of the crust and upper mantle, Geophys. J. Int., 151, 1–18, 2002.
Song, T. A., Helmberger, D. V., and Grand, S. P.: Low-velocity zone atop the 410 km seismic discontinuity, Nature, 427, 530–533, 2004.
Somali, Z. H., Roberts, R. G., Pedersen, L. B., and the TOR Working Group: Lithospheric structure of the Tornquist Zone resolved by nonlinear P and S teleseismic tomography along the TOR array, Tectonophys, 416, 133–149, 2006.
Świeczak, M., Grad, M., and TOR and SVEKALAPKO Working Groups: upper mantle seismic discontinuities: topography variations beneath Eastern Europe, Acta Geophys. Pol., 52, 251–270, 2004.
Thybo, H. and Perchuc, E.: The seismic 8° discontinuity and partial melting in continental mantle, Science, 275, 1626–1629, 1997.
Thybo, H., Perchuc, E., and Pavlenkova, N.: Two Reflectors in the 400 km Depth Range Revealed from Peaceful Nuclear Explosion Seismic Sections, Upper Mantle Heterogeneities from Active and Passive Seismology, edited by: Fuchs, K., NATO ASI Series, 97–104, 1997.
Torsvik, T. H., Smethurst, M. A., Meert, J. G., Van der Voo, R., McKerrow, W. S., Brasier, M. D., Sturt, B. A., and Walderhaug. H. J.: Continental break-up and collision in the Neoproterozoic and Palaeozoic: a tale of Baltica and Laurentia, Earth-Sci. Rev., 40, 229–258, 1996.
Torsvik, T. H. and Rehnström, E. F.: The Tornquist Sea and Baltica-Avalonia docking, Tectonophys, 362, 67–82, 2003.

SED
6, 559–598, 2014

Wessel, P. and Smith, W. H. F.: New version of Generic Mapping Tools released, EOS, 76, 453, 1995.

Wilde-Piórko, M.: Crustal structure from seismic receiver function, Przegląd Geofizyczny, 1–2, 31–45, 2005.

Wilde-Piórko, M., Geissler, W., Plomerová, J., Grad, M., Babuška, V., Brückl, E., Cyziene, J., Czuba, W., England, R., Gaczyński, E., Gazdova, R., Gregersen, S., Guterch, A., Hanka, W., Hegedűs, E., Heuer, B., Jedlička, P., Lazauskiene, J., Keller, G., Kind, R., Klinge, K., Kolinsky, P., Komminaho, K., Kozlovskaya, E., Krüger, F., Larsen, T., Majdański, M., Malek, J., Motuza, G., Novotný, O., Pietrasiak, R., Plenefisch, T., Růžek, B., Sliaupa, S., Środa, P., Świeczak, M., Tiira, T., Voss, P., and Wiejacz, P.: PASSEQ 2006–2008: Passive seismic experiment in Trans-European Suture Zone, Studia Geophysica et Geodetica, 52, 439–448, 2008.

Xu, W., Lithgow-Bertelloni, C., Stixrude, L., and Ritsema, J.: The effect of bulk composition and temperature on mantle seismic structure, Earth Planet. Sci. Lett., 275, 70–79, 2008.

Zelt, C.: ZPLOT – an iteractive plotting and picking program for seismic data, Bullard Lab. Univ. of Cambridge, Cambridge UK, 1994.

Ziegler, P. A. and Dèzes, P.: Crustal configuration of Western and Central Europe, in: European Lithosphere Dynamics, edited by: Gee, D. G. and Stephenson, R. A., Geol. Soc., London, Memoirs 32, 43–56, 2006.

Znosko, J.: Polish Caledonides and their relation to other European Caledonides, Ann. Soc. Geol. Pol., 56, 33–52, 1986.

SED
6, 559–598, 2014

Table 1. List of seismic events shown in Fig. 1. Numbers from column 1 correspond to numbers of seismic records in Fig. 1.

No	Offset (km)	Date	Origin time (UTC)	Lat	Long	Depth (km)	Mag (mb)	Seismic region
1	2259.18	24 Jun 2002	01:20:37.60	35.92	9.88	10.0	4.7	Tunisia
2	2267.73	25 Feb 2007	21:53:13.80	73.18	6.77	10.0	5.1	Greenland Sea
3	2275.16	07 Jun 1999	16:10:33.66	73.02	5.35	10.0	5.2	Greenland Sea
4	2307.27	30 Aug 2005	20:53:48.17	71.91	−1.09	10.0	4.8	Jan Mayen Island region
5	2322.30	08 Sep 2008	21:17:15.10	72.63	0.96	10.0	5.0	Norwegian Sea
6	2323.20	26 Aug 1999	05:03:05.04	71.70	−2.43	10.0	5.1	Jan Mayen Island region
7	2334.51	02 Dec 1997	00:02:03.51	71.65	−3.03	10.0	5.0	Jan Mayen Island region
8	2340.29	13 Aug 2006	19:03:08.50	71.39	−4.00	13.1	4.8	Jan Mayen Island region
9	2360.94	23 Mar 1998	20:19:27.74	71.50	−4.47	10.0	5.1	Jan Mayen Island region
10	2392.71	22 May 2003	13:57:21.27	37.12	3.84	10.0	4.8	Western Mediterranean Sea
11	2395.07	16 Nov 2000	11:33:08.87	36.63	4.79	8.7	4.8	Northern Algeria
12	2402.14	22 May 2003	03:14:04.85	37.16	3.57	15.0	5.2	Western Mediterranean Sea
13	2412.09	02 Sep 2008	20:00:50.82	38.72	45.79	3.0	4.9	Iran–Armenia–Azerbaijan border
14	2421.17	19 Jun 2003	12:59:23.14	71.08	−7.64	0.5	5.6	Jan Mayen Island region
15	2422.18	14 Apr 2004	23:07:37.81	71.05	−7.74	10.5	5.7	Jan Mayen Island region
16	2424.21	27 May 2003	17:11:28.35	36.94	3.54	6.1	5.5	Northern Algeria
17	2430.11	18 Aug 2000	18:15:06.54	36.19	4.96	10.0	4.9	Northern Algeria

SED
6, 559–598, 2014

Table 2. Mean signal-to-noise ratio for the analysed groups of events.

Region	Number of events	Signal to noise ratio		
		Raw data	After filtering (0.5–2.0 Hz)	Improvement (%)
JMR	34	4.70	8.17	73.83
CR 020	34	2.57	7.50	191.83
CR 2050	23	3.52	6.66	89.20
CR 50+	12	5.54	12.66	128.52
GTR 020	53	6.59	4.85	−26.40
GTR 2050	36	3.61	5.26	45.71
GTR 50+	14	13.84	18.02	30.20
WMSR	43	6.30	11.54	83.17
Average		5.38	8.16	67.76

SED
6, 559–598, 2014

Table 3. The MP1-SUW *P* wave velocity model.

Depth (km)	*P* wave velocity (km s^{-1})	Depth (km)	*P* wave velocity (km s^{-1})
0	5.60	160	8.20
5	6.00	170	8.20
10	6.05	170	8.18
15	6.10	180	8.18
30	6.20	180	8.20
30	6.60	190	8.18
44	7.20	190	8.20
44	8.15	200	8.20
105	8.35	200	8.18
105	8.20	210	8.18
110	8.20	210	8.20
110	8.18	220	8.20
120	8.18	220	8.45
120	8.20	335	8.60
130	8.20	335	8.85
130	8.18	430	9.05
140	8.18	430	8.60
140	8.20	440	8.60
150	8.20	440	9.60
150	8.18	620	10.10
160	8.18		

SED
6, 559–598, 2014

Table 4. Statistics of the traveltime residuals for the MP1-SUW model (in bold) and the AK135.

Region	Number of events	Standard deviation	Variation	Kurtosis	RMS
Greece and Turkey region	103	1.01	1.01	4.46	1.00
		1.99	3.96	3.62	2.25
Greece and Turkey 0–20	53	**0.85**	**0.73**	**3.32**	**0.88**
		1.80	3.25	3.74	3.03
Greece and Turkey 20–50	36	**1.10**	**1.22**	**6.18**	**1.10**
		1.40	1.96	3.76	1.43
Greece and Turkey 50+	14	**1.18**	**1.40**	**2.69**	**1.20**
		1.29	1.65	2.76	1.44
Caucasus region	69	1.50	2.26	3.45	1.46
		1.61	2.59	2.79	1.65
Caucasus 0–20	34	**1.67**	**2.78**	**2.33**	**1.64**
		1.86	3.44	2.21	1.87
Caucasus 20–50	23	**1.58**	**2.51**	**4.38**	**1.55**
		1.55	2.40	3.52	1.59
Caucasus 50+	12	**0.77**	**0.60**	**3.08**	**0.74**
		0.86	0.73	3.65	1.13
Western Mediterranean Sea region	43	1.20	1.44	3.57	1.19
		1.57	2.46	2.15	1.63
Jan Mayen region	34	0.32	0.10	2.22	0.36
		0.27	0.07	2.63	0.29
All events	249	1.08	1.31	3.72	1.07
		1.58	2.79	3.00	1.71
$P_{335}P$	83	**0.75**	**0.56**	**3.91**	**0.75**
$P_{440}P$	76	**0.75**	**0.57**	**4.00**	**0.80**

SED
6, 559–598, 2014

Table A1. Western Mediterranean Sea Region.

No	Date	UTC (origin time)	Latitude	Longitude	Depth (km)	Magnitude (mb)	Seismic region
1	04 Sep 1996	04:14:04	36.97	2.90	16.0	5.3	Northern Algeria
2	21 Dec 1996	08:46:01	40.00	13.05	481.6	5.1	Tyrrhenian Sea
3	20 Mar 1997	18:02:18	34.00	8.24	13.6	5.0	Tunisia
4	21 May 1997	23:49:42	42.85	−7.15	9.0	4.7	Spain
5	21 May 1997	23:50:43	42.86	−7.16	13.0	5.2	Spain
6	22 May 1997	00:17:18	42.84	−7.13	17.0	4.7	Spain
7	20 Jun 1998	02:25:47	38.44	12.78	5.0	4.9	Sicily
8	14 Sep 1998	05:24:47	38.55	13.46	5.0	4.9	Sicily
9	02 Feb 1999	13:45:16	38.14	−1.56	2.9	4.7	Spain
10	23 Oct 1999	02:06:01	38.88	14.68	308.5	4.7	Sicily
11	22 Dec 1999	17:36:56	35.29	−1.32	10.0	5.3	Northern Algeria
12	18 Aug 2000	18:15:07	36.19	4.96	10.0	4.9	Northern Algeria
13	10 Nov 2000	20:10:53	36.55	4.77	10.0	5.8	Northern Algeria
14	16 Nov 2000	11:33:09	36.63	4.79	8.7	4.8	Northern Algeria
15	17 May 2001	11:43:58	38.96	15.53	239.3	4.9	Sicily
16	25 Nov 2001	19:34:18	37.78	13.99	5.0	5.1	Sicily
17	04 Feb 2002	20:09:30	37.17	−2.67	11.2	4.9	Spain
18	24 Jun 2002	01:20:38	35.92	9.88	10.0	4.7	Tunisia
19	06 Aug 2002	06:16:19	38.10	−2.00	10.0	4.6	Spain
20	06 Sep 2002	01:21:27	38.36	13.69	9.6	5.8	Sicily
21	27 Oct 2002	02:50:28	37.79	15.16	20.6	4.6	Sicily
22	21 May 2003	18:44:20	36.99	3.66	13.4	6.3	Northern Algeria
23	22 May 2003	13:57:21	37.12	3.84	10.0	4.8	Western Mediterranean Sea
24	22 May 2003	03:14:05	37.16	3.57	15.0	5.2	Western Mediterranean Sea
25	27 May 2003	17:11:28	36.94	3.54	6.1	5.5	Northern Algeria
26	29 May 2003	02:15:01	36.90	3.26	15.0	4.8	Northern Algeria
27	24 Feb 2004	02:27:46	35.26	−4.00	8.9	6.0	Strait of Gibraltar
28	07 Mar 2004	06:37:52	35.18	−4.09	11.0	4.7	Strait of Gibraltar
29	05 May 2004	13:39:43	38.55	14.79	228.6	5.4	Sicily
30	07 Feb 2005	20:05:37	36.23	10.91	10.0	4.7	Tunisia
31	07 Feb 2005	20:46:26	36.23	10.85	14.2	5.0	Tunisia
32	09 Mar 2005	18:23:41	35.50	5.57	10.0	4.6	Northern Algeria
33	02 Apr 2006	06:44:32	35.03	3.72	10.0	4.7	Northern Algeria
34	23 Jul 2006	20:17:16	35.93	0.62	10.0	4.5	Northern Algeria
35	26 Oct 2006	14:28:38	38.76	15.40	219.2	5.7	Sicily
36	05 Nov 2006	17:15:01	39.80	13.77	428.5	4.7	Tyrrhenian Sea
37	30 Dec 2006	23:50:49	34.92	3.31	10.0	4.8	Northern Algeria
38	09 Jan 2008	22:24:04	35.62	−0.58	10.0	4.6	Northern Algeria
39	06 Jun 2008	20:02:57	35.88	−0.66	4.0	5.5	Northern Algeria
40	18 Jun 2008	13:23:59	36.23	1.08	5.0	4.6	Northern Algeria
41	14 Dec 2009	06:41:11	33.02	−0.09	0.0	4.6	Northern Algeria
42	11 Apr 2010	22:08:10	37.08	−3.47	10.0	6.2*	Spain
43	14 May 2010	12:29:22	35.90	4.03	2.0	5.1	Northern Algeria

* magnitude other than mb

SED
6, 559–598, 2014

Table A2. Jan Mayen Region.

No	Date	UTC (origin time)	Latitude	Longitude	Depth (km)	Magnitude (mb)	Seismic region
1	22 Jul 1997	16:21:41.30	66.31	−18.40	10.0	4.7	Iceland region
2	02 Dec 1997	00:02:03.51	71.65	−3.03	10.0	5.0	Jan Mayen Island region
3	13 Dec 1997	07:02:03.89	71.24	−8.34	10.0	5.2	Jan Mayen Island region
4	23 Mar 1998	20:19:27.74	71.50	−4.47	10.0	5.1	Jan Mayen Island region
5	04 Jun 1998	21:36:54.42	63.95	−21.28	10.0	5.1	Iceland region
6	07 Jun 1999	16:10:33.66	73.02	5.35	10.0	5.2	Greenland Sea
7	01 Jul 1999	02:06:58.37	70.43	−15.03	10.0	4.9	Jan Mayen Island region
8	01 Jul 1999	03:20:42.76	70.40	−15.12	10.0	4.8	Jan Mayen Island region
9	26 Aug 1999	05:03:05.04	71.70	−2.43	10.0	5.1	Jan Mayen Island region
10	03 Feb 2000	15:53:13.12	75.25	10.25	10.0	5.5	Svalbard region
11	21 May 2000	19:58:47.59	71.19	−8.22	10.0	5.3	Jan Mayen Island region
12	24 May 2000	01:10:50.95	71.24	−8.69	10.0	5.2	Jan Mayen Island region
13	17 Jun 2000	15:40:41.93	63.92	−20.47	10.0	5.7	Iceland
14	21 Jun 2000	00:51:47.04	63.91	−20.74	10.0	6.0	Iceland
15	21 Jun 2000	14:56:25.39	70.77	−13.60	10.0	4.9	Jan Mayen Island region
16	09 Jul 2000	02:18:30.21	70.79	−13.51	10.0	4.7	Jan Mayen Island region
17	29 Jul 2000	22:30:13.01	70.87	−13.15	10.0	4.7	Jan Mayen Island region
18	10 Jul 2002	14:13:11.07	73.12	5.26	10.0	4.8	Greenland Sea
19	12 Oct 2002	03:46:47.50	71.56	−2.83	10.0	4.7	Jan Mayen Island region
20	19 Jun 2003	12:59:23.14	71.08	−7.64	0.5	5.6	Jan Mayen Island region
21	14 Apr 2004	23:07:37.81	71.05	−7.74	10.5	5.7	Jan Mayen Island region
22	25 Jul 2005	16:02:06.68	71.10	−7.57	15.3	5.3	Jan Mayen Island region
23	30 Aug 2005	20:53:48.17	71.91	−1.09	10.0	4.8	Jan Mayen Island region
24	07 Nov 2005	01:49:34.68	71.69	−12.15	10.0	4.8	Jan Mayen Island region
25	28 May 2006	13:23:28.69	74.09	13.78	10.0	5.0	Norwegian Sea
26	30 Jul 2006	07:16:56.14	72.18	0.84	10.0	4.9	Norwegian Sea
27	13 Aug 2006	19:03:08.50	71.39	−4.00	13.1	4.8	Jan Mayen Island region
28	25 Feb 2007	21:53:13.80	73.18	6.77	10.0	5.1	Greenland Sea
29	06 May 2008	19:51:10.10	71.46	−12.27	10.0	4.7	Jan Mayen Island region
30	29 May 2008	15:45:58.90	64.01	−21.02	2.0	5.9	Iceland
31	08 Sep 2008	21:17:15.10	72.63	0.96	10.0	5.0	Norwegian Sea
32	28 Sep 2008	22:20:19.40	71.30	−4.21	10.0	5.4	Jan Mayen Island region
33	29 Sep 2008	19:20:19.60	71.55	−4.01	10.0	5.0	Jan Mayen Island region
34	20 Aug 2009	06:35:03.90	72.26	0.97	10.0	5.8	Norwegian Sea

SED
6, 559–598, 2014

Table A3. Caucasus Region.

No	Date	UTC (origin time)	Latitude	Longitude	Depth (km)	Magnitude (mb)	Seismic region
1	05 Dec 1995	18:52:38.32	39.60	40.26	10.0	5.2	Turkey
2	13 Apr 1998	15:14:31.75	39.31	41.07	15.3	4.8	Turkey
3	05 Oct 1998	02:20:31.61	33.24	47.24	18.1	5.2	Western Iran
4	03 Dec 1999	17:06:54.24	40.41	42.36	13.1	5.3	Turkey
5	01 Sep 2001	22:38:18.09	32.83	47.68	17.0	5.0	Iran–Iraq border region
6	24 Apr 2002	19:48:04.15	34.64	47.40	10.0	5.3	Western Iran
7	22 Jun 2002	02:58:21.47	35.59	49.02	10.0	6.2	Western Iran
8	02 Sep 2002	01:00:03.58	35.70	48.83	10.0	5.1	Western Iran
9	27 Jan 2003	05:26:23.11	39.48	39.85	10.0	5.5	Turkey
10	01 May 2003	00:27:04.73	39.00	40.46	10.0	5.7	Turkey
11	25 Mar 2004	19:30:47.79	39.93	40.88	10.0	5.0	Turkey
12	28 Mar 2004	03:51:08.85	39.95	40.96	5.0	5.2	Turkey
13	28 May 2004	12:38:43.04	36.32	51.59	17.0	6.2	Northern and central Iran
14	01 Jul 2004	22:30:08.03	39.78	43.97	5.0	5.3	Turkey
15	12 Mar 2005	07:36:10.21	39.39	40.94	8.3	5.3	Turkey
16	14 Mar 2005	01:55:56.68	39.33	40.91	9.4	5.4	Turkey
17	23 Mar 2005	21:44:52.07	39.40	40.88	13.2	5.1	Turkey
18	06 Jun 2005	07:41:27.70	39.30	41.02	3.2	4.9	Turkey
19	26 Sep 2005	18:57:02.89	37.33	47.71	10.0	5.0	Northwestern Iran
20	10 Dec 2005	00:09:47.90	39.37	40.94	5.1	5.0	Turkey
21	30 Mar 2006	19:36:18.17	33.56	48.75	15.7	5.0	Western Iran
22	31 Mar 2006	01:17:02.56	33.58	48.80	15.4	5.7	Western Iran
23	31 Mar 2006	11:54:02.96	33.63	48.68	15.8	4.8	Western Iran
24	02 Jul 2006	19:39:41.56	39.33	40.93	18.0	4.6	Turkey
25	21 Jan 2007	07:38:59.13	39.60	42.89	8.8	5.0	Turkey
26	18 Jun 2007	14:29:49.77	34.50	50.87	11.0	5.3	Northern and central Iran
27	25 Aug 2007	22:05:49.37	39.27	41.14	7.4	5.0	Turkey
28	02 Sep 2008	20:00:50.82	38.72	45.79	3.0	4.9	Iran–Armenia–Azerbaijan border region
29	11 Oct 2008	09:06:10.77	43.37	46.25	16.0	5.6	Eastern Caucasus
30	11 Oct 2008	09:22:01.21	43.34	46.19	10.0	5.2	Eastern Caucasus
31	01 Dec 2008	10:18:38	35.44	46.11	0	5.0	Iran–Iraq border region
32	18 Jul 2009	20:32:27.60	35.85	43.35	7.0	5.2	Iraq
33	07 Sep 2009	22:41:37.40	42.67	43.43	15.0	5.7	Western Caucasus
34	13 Oct 2009	00:54:26.40	34.94	46.89	10.0	5.1	Western Iran
35	05 Dec 1995	18:49:32.05	39.43	40.11	25.5	5.3	Turkey
36	28 Feb 1997	12:57:22.78	38.09	48.04	39.2	5.5	Iran–Armenia–Azerbaijan border region
37	27 Nov 1997	17:34:29.70	41.86	45.37	29.5	5.1	Eastern Caucasus
38	21 Aug 1998	05:13:12.52	34.13	48.16	47.4	4.9	Western Iran
39	04 Oct 1998	00:42:50.00	33.23	47.20	24.9	5.2	Western Iran
40	31 Jan 1999	05:07:14.13	43.25	46.90	35.5	5.3	Eastern Caucasus
41	26 Feb 2000	08:18:37.97	37.31	44.77	34.2	4.6	Turkey–Iran border region
42	15 Nov 2000	15:05:36.62	38.41	42.95	48.4	5.2	Turkey
43	25 Nov 2000	18:10:46.19	40.19	49.95	22.2	6.2	Eastern Caucasus
44	07 Jan 2001	06:49:01.97	40.17	50.12	43.6	4.8	Caspian Sea
45	23 Mar 2001	05:24:12.01	32.88	46.60	34.5	5.1	Iran–Iraq border region
46	05 Jun 2001	15:33:28.17	42.41	48.70	48.4	5.0	Caspian Sea
47	10 Jul 2001	21:42:07.63	39.81	41.64	22.5	4.9	Turkey

SED
6, 559–598, 2014

Table A3. Continued.

No	Date	UTC (origin time)	Latitude	Longitude	Depth (km)	Magnitude (mb)	Seismic region
48	19 Apr 2002	13:46:50.62	36.52	49.77	38.8	5.2	Western Iran
49	18 Jun 2002	03:19:24.18	33.24	45.91	36.3	5.0	Iran–Iraq border region
50	09 Nov 2002	02:18:14.85	44.93	37.76	33.8	5.0	Western Caucasus
51	24 Dec 2002	17:03:03.92	34.49	47.45	44.9	5.0	Western Iran
52	21 Nov 2004	21:37:22.23	33.14	47.90	30.1	4.9	Western Iran
53	22 Nov 2004	04:01:28.34	33.21	47.92	34.1	5.0	Western Iran
54	25 Jan 2005	11:39:19.62	33.44	45.86	48.6	4.8	Iran–Iraq border region
55	25 Jan 2005	16:44:12.18	37.57	43.68	22.0	5.3	Turkey
56	06 Feb 2006	04:08:03.95	42.65	43.50	23.5	5.0	Western Caucasus
57	11 Jul 2007	06:51:15.00	38.82	48.64	28.6	4.9	Iran–Armenia–Azerbaijan border region
58	03 Jan 1996	08:42:26.35	38.96	48.70	62.9	4.9	Iran–Armenia–Azerbaijan border region
59	22 Apr 1996	14:42:37.14	39.19	47.33	70.4	4.9	Iran–Armenia–Azerbaijan border region
60	02 Mar 1997	18:29:48.60	38.00	47.89	55.9	5.0	Northwestern Iran
61	09 Jul 1998	14:19:21.68	38.69	48.48	55.4	5.8	Iran–Armenia–Azerbaijan border region
62	05 Aug 1998	14:27:02.25	33.13	46.22	53.0	4.9	Iran–Iraq border region
63	15 Jan 1999	19:14:13.13	35.25	45.13	59.2	5.0	Iran–Iraq border region
64	21 Feb 1999	18:14:36.42	43.26	46.91	51.2	5.0	Eastern Caucasus
65	04 Jun 1999	09:12:51.80	40.76	47.46	51.5	5.4	Eastern Caucasus
66	21 Mar 2000	14:07:43.26	40.05	48.20	77.6	5.0	Eastern Caucasus
67	25 Nov 2000	18:09:11.53	40.22	49.94	51.0	5.7	Eastern Caucasus
68	29 Nov 2000	10:45:03.39	39.97	50.09	71.7	4.3	Caspian Sea
69	11 Feb 2002	16:18:34.09	40.03	50.18	56.9	4.8	Caspian Sea

SED
6, 559–598, 2014

Table A4. Greece and Turkey Region

No	Date	UTC (origin time)	Latitude	Longitude	Depth (km)	Magnitude (mb)	Seismic region
1	14 Feb 2000	06:56:34.69	41.04	31.74	10.0	4.8	Turkey
2	22 Feb 2000	11:55:22.38	34.48	25.55	9.7	5.1	Crete
3	10 Mar 2000	22:01:45.63	34.26	26.02	10.0	5.2	Crete
4	21 Apr 2000	12:23:09.02	37.88	29.36	19.9	4.8	Turkey
5	24 May 2000	05:40:36.05	35.97	21.99	19.9	5.3	Central Mediterranean Sea
6	06 Jun 2000	02:41:50.06	40.70	32.98	10.0	5.5	Turkey
7	13 Jun 2000	01:43:14.69	35.12	27.07	9.8	5.1	Dodecanese Islands
8	23 Aug 2000	13:41:26.95	40.78	30.76	10.5	5.1	Turkey
9	15 Dec 2000	16:44:46.64	38.40	31.33	10.0	5.1	Turkey
10	29 May 2001	04:43:57.06	35.38	27.75	11.0	5.0	Dodecanese Islands
11	22 Jun 2001	11:54:50.78	39.34	27.91	7.0	4.6	Turkey
12	26 Jul 2001	00:21:38.63	39.10	24.27	19.0	5.8	Aegean Sea
13	26 Aug 2001	00:41:12.81	40.96	31.54	8.8	4.9	Turkey
14	16 Sep 2001	02:00:47.29	37.26	21.93	10.1	5.3	Southern Greece
15	30 Oct 2001	21:00:05.41	35.87	29.77	5.0	4.6	Eastern Mediterranean Sea
16	12 Oct 2002	05:58:50.44	34.76	26.38	12.2	5.1	Crete
17	10 Apr 2003	00:40:15.95	38.25	26.89	11.3	5.3	Aegean Sea
18	17 Apr 2003	22:34:26.29	38.19	26.95	19.6	4.7	Aegean Sea
19	06 Jul 2003	19:10:27.99	40.45	26.04	17.1	5.1	Turkey
20	06 Jul 2003	20:10:15.93	40.43	26.07	17.0	4.9	Turkey
21	07 Feb 2004	21:17:21.37	35.83	26.86	14.1	5.2	Crete
22	01 Mar 2004	00:35:56.90	37.17	22.12	13.6	5.3	Southern Greece
23	17 Mar 2004	05:20:57.75	34.66	23.39	14.7	5.9	Crete
24	15 Jun 2004	12:02:37.57	40.41	25.85	7.1	4.6	Aegean Sea
25	03 Aug 2004	13:11:30.99	36.86	27.78	10.0	4.8	Dodecanese Islands
26	04 Aug 2004	14:18:48.59	36.84	27.78	10.0	4.9	Dodecanese Islands
27	04 Aug 2004	03:01:05.92	36.84	27.77	10.0	5.2	Dodecanese Islands
28	04 Aug 2004	04:19:46.55	36.83	27.82	10.0	5.2	Dodecanese Islands
29	10 Jan 2005	23:48:49.61	36.86	27.93	17.0	5.0	Dodecanese Islands
30	11 Jan 2005	04:35:56.88	36.90	27.88	18.4	5.0	Dodecanese Islands
31	30 Jul 2005	21:45:02.07	39.41	33.10	15.7	4.7	Turkey
32	04 Aug 2005	10:45:28.68	34.83	26.51	10.0	4.7	Crete
33	17 Sep 2005	09:46:56.24	38.19	26.71	14.8	5.3	Aegean Sea
34	17 Oct 2005	09:55:30.53	38.18	26.71	15.1	4.8	Aegean Sea
35	17 Oct 2005	05:45:16.56	38.10	26.66	5.3	5.0	Aegean Sea
36	20 Oct 2005	21:40:02.09	38.11	26.73	10.0	5.4	Aegean Sea
37	24 Sep 2006	14:00:22.74	40.48	29.04	14.1	4.7	Turkey
38	10 Apr 2007	22:00:36.81	37.94	30.96	18.6	4.6	Turkey
39	21 May 2007	16:39:10.12	35.06	27.74	19.6	4.7	Dodecanese Islands
40	31 Aug 2007	20:52:42.69	36.64	26.26	18.2	4.9	Dodecanese Islands
41	23 Sep 2007	00:54:29.48	35.11	27.07	12.0	5.1	Dodecanese Islands
42	09 Nov 2007	01:43:05.13	38.77	25.71	13.1	4.9	Aegean Sea
43	20 Dec 2007	09:48:30.43	39.43	33.15	11.3	5.1	Turkey
44	26 Dec 2007	23:47:11.43	39.44	33.11	10.8	5.1	Turkey
45	20 Feb 2008	18:27:07.02	36.30	21.78	17.4	5.7	Southern Greece
46	26 Feb 2008	10:46:08.35	35.93	21.80	10.0	4.9	Central Mediterranean Sea
47	25 Apr 2008	04:48:57.10	37.82	29.30	10.0	4.6	Turkey
48	21 Jun 2008	05:57:16.20	36.10	21.93	17.0	4.8*	Southern Greece
49	21 Jun 2008	11:36:23.90	36.06	21.82	5.0	5.4	Southern Greece
50	12 Nov 2008	14:03:18.31	38.84	35.52	10.0	4.8	Turkey
51	17 Feb 2009	05:28:19.00	39.11	29.04	7.3	4.8	Turkey
52	01 Jul 2009	09:30:10.50	34.20	25.45	19.0	6.1	Crete
53	04 Dec 2009	06:02:19.00	37.92	28.73	5.0	5.1	Turkey

SED
6, 559–598, 2014

Table A4. Continued.

No	Date	UTC (origin time)	Latitude	Longitude	Depth (km)	Magnitude (mb)	Seismic region
54	05 Apr 2000	04:36:57.51	34.42	25.79	33.0	5.3	Crete
55	24 May 2000	10:01:43.76	35.95	22.04	20.5	4.8	Central Mediterranean Sea
56	01 May 2001	06:00:56.04	35.67	27.47	28.5	5.1	Dodecanese Islands
57	10 Jun 2001	13:11:04.17	38.54	25.59	32.0	5.1	Aegean Sea
58	23 Jun 2001	06:52:42.67	35.54	28.11	45.5	5.3	Eastern Mediterranean Sea
59	26 Nov 2001	05:03:21.06	34.82	24.30	33.0	5.3	Crete
60	03 Feb 2002	07:11:31.47	38.52	31.20	22.1	5.6	Turkey
61	03 Feb 2002	07:14:39.81	38.72	30.89	35.4	5.1	Turkey
62	03 Feb 2002	09:26:45.55	38.63	30.88	24.9	5.6	Turkey
63	03 Feb 2002	11:39:58.73	38.56	31.08	31.0	5.0	Turkey
64	03 Feb 2002	11:54:38.45	38.59	31.06	30.1	4.8	Turkey
65	23 Jul 2003	04:56:05.18	38.05	28.89	28.3	4.8	Turkey
66	26 Jul 2003	08:36:50.87	38.06	28.91	21.3	5.1	Turkey
67	17 Oct 2003	12:57:07.13	35.97	22.19	30.0	5.5	Central Mediterranean Sea
68	20 Dec 2004	23:02:14.98	36.94	28.36	25.5	5.1	Dodecanese Islands
69	10 Jan 2005	23:50:27.87	36.94	27.89	38.6	4.8	Dodecanese Islands
70	23 Jan 2005	22:36:07.39	35.85	29.66	42.4	5.4	Eastern Mediterranean Sea
71	30 Jan 2005	16:23:49.69	35.81	29.71	43.7	5.0	Eastern Mediterranean Sea
72	25 Nov 2005	09:30:55.23	35.08	23.51	33.0	5.2	Crete
73	09 Apr 2006	23:27:19.53	35.18	27.25	30.6	5.1	Dodecanese Islands
74	13 Aug 2006	10:35:12.38	34.36	26.56	33.2	5.2	Crete
75	22 Aug 2006	09:23:21.62	35.08	27.09	49.9	5.0	Dodecanese Islands
76	29 Oct 2007	09:23:19.29	36.92	29.33	36.9	4.9	Turkey
77	16 Nov 2007	09:08:27.28	36.89	29.35	29.4	4.7	Turkey
78	14 Feb 2008	10:09:23.17	36.52	21.67	31.5	6.2	Southern Greece
79	14 Feb 2008	12:08:57.10	36.38	21.83	35.3	5.9	Southern Greece
80	19 Feb 2008	23:15:43.73	36.31	21.81	35.3	4.9	Southern Greece
81	28 Mar 2008	00:16:20.54	34.79	25.34	48.9	5.3	Crete
82	10 May 2008	20:52:58.22	36.53	22.43	33.0	4.9*	Southern Greece
83	12 Jun 2008	00:20:45.60	35.11	26.19	29.0	5.0*	Crete
84	03 Aug 2008	00:39:16.10	39.59	23.90	30.0	5.3*	Aegean Sea
85	04 Aug 2008	19:38:22.80	33.89	26.56	32.0	5.0*	Eastern Mediterranean Sea
86	14 Oct 2008	02:06:34.70	38.85	23.62	24.0	4.9	Greece
87	13 Dec 2008	08:27:19.20	38.72	22.57	24.0	5.1	Greece
88	28 Dec 2008	22:58:59.00	40.39	25.78	35.0	5.1	Aegean Sea
89	13 Jan 2009	06:12:42.90	35.66	26.39	42.0	5.1	Crete
90	22 Jan 2002	04:53:52.10	35.57	26.63	94.6	6.1	Crete
91	21 May 2002	20:53:30.18	36.64	24.27	106.7	5.4	Southern Greece
92	06 Jun 2002	22:35:41.51	35.53	26.16	95.2	4.8	Crete
93	03 May 2003	11:22:40.69	36.89	31.53	133.0	4.9	Turkey
94	13 Sep 2003	13:46:14.54	36.62	26.87	153.0	5.0	Dodecanese Islands
95	07 Oct 2004	01:05:12.23	36.47	26.79	133.9	5.5	Dodecanese Islands
96	04 Nov 2004	06:22:37.56	35.96	23.15	70.1	5.4	Crete
97	14 May 2005	23:46:48.31	35.66	31.54	59.7	4.9	Cyprus region
98	08 Jan 2006	11:34:54.64	36.28	23.27	58.4	6.5	Southern Greece
99	03 Feb 2007	13:43:22.50	35.81	22.49	53.0	5.4	Central Mediterranean Sea
100	06 Jan 2008	05:14:21.03	37.26	22.70	83.8	6.0	Southern Greece
101	15 Jul 2008	03:26:34.50	35.85	27.92	56.0	6.2*	Dodecanese Islands
102	14 May 2009	09:13:41.70	36.02	27.01	106.0	4.9	Crete
103	22 Dec 2009	06:06:26.10	35.92	31.44	81.0	5.1	Cyprus region

* magnitude other than mb

SED
6, 559–598, 2014

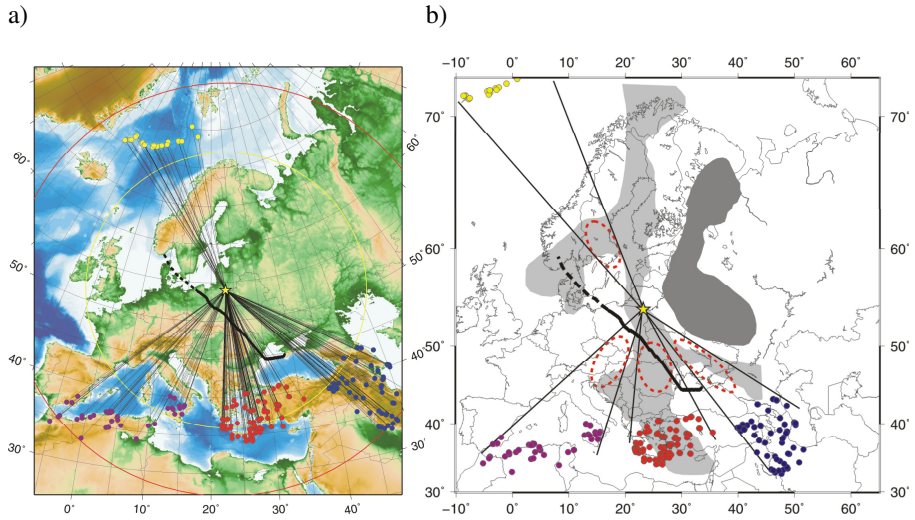

Figure 1. (a) Four groups of earthquakes recorded at the SUW station (yellow asterisk): JMR (yellow points), WMSR (violet points), GTR (red points) and CR (blue points). Circles centred at SUW mark the distance of 2000 km (yellow) and 3000 km (red). Thick black line represents the Teisseyre – Tornquist Zone (TTZ). **(b)** Map of the study area with indication of the regions to which our upper mantle model pertains (red dashed ellipses). Areas shaded in grey are characterized by higher S wave velocities at 250 km depth according to model of Shapiro and Ritzwoller (2002). Light grey represents velocities about 4.65 km s^{-1} and dark grey about 4.80 km s^{-1}.

SED
6, 559–598, 2014

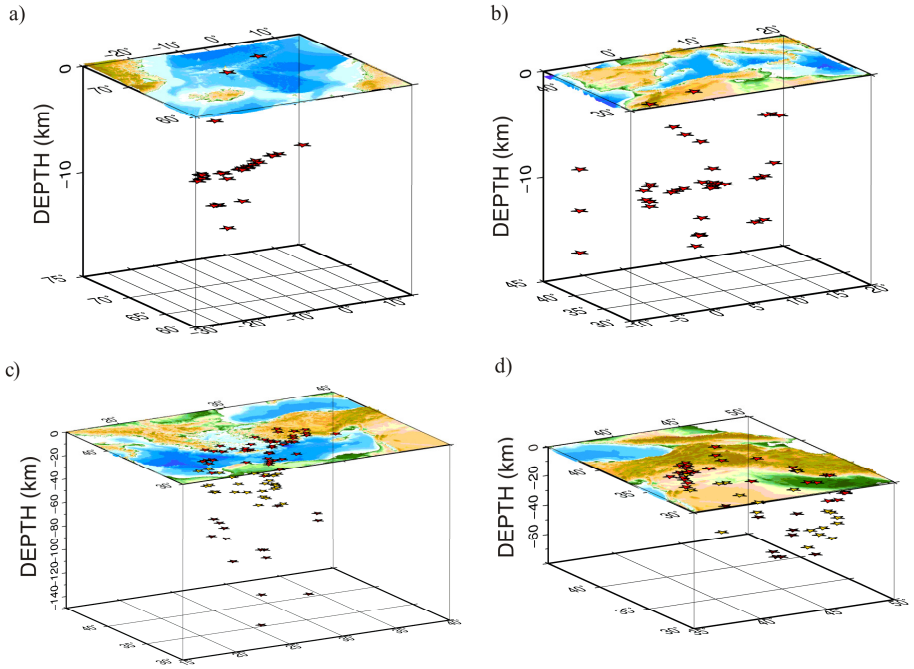

Figure 2. Distribution of the focal depths for the analyzed groups of earthquakes: **(a)** JMR, **(b)** WMSR, **(c)** GTR, **(d)** CR.

SED
6, 559–598, 2014

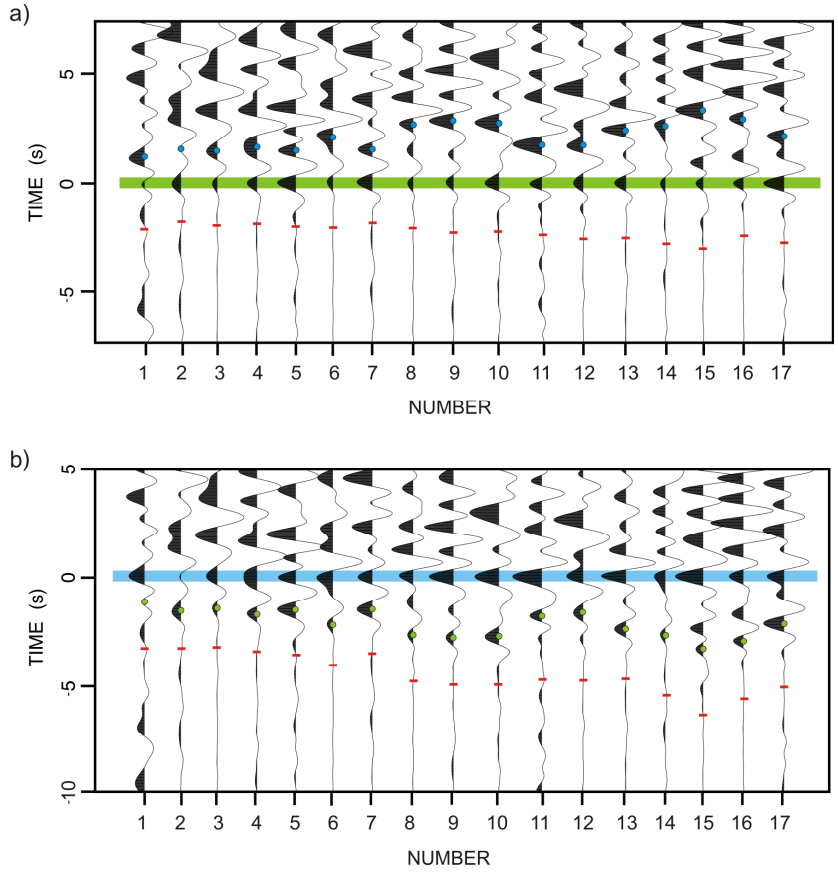

Figure 3. Seismograms aligned by the maximum amplitudes of: **(a)** $P_{410}P$ (green line), **(b)** $P_{335}P$ (blue line). Seismograms are ordered by event's number (see Table 1). Red dashes represent first arrivals. Blue dots in **(a)** correspond to blue line in **(b)**. Green dots in **(b)** correspond to green line in **(a)**.

SED
6, 559–598, 2014

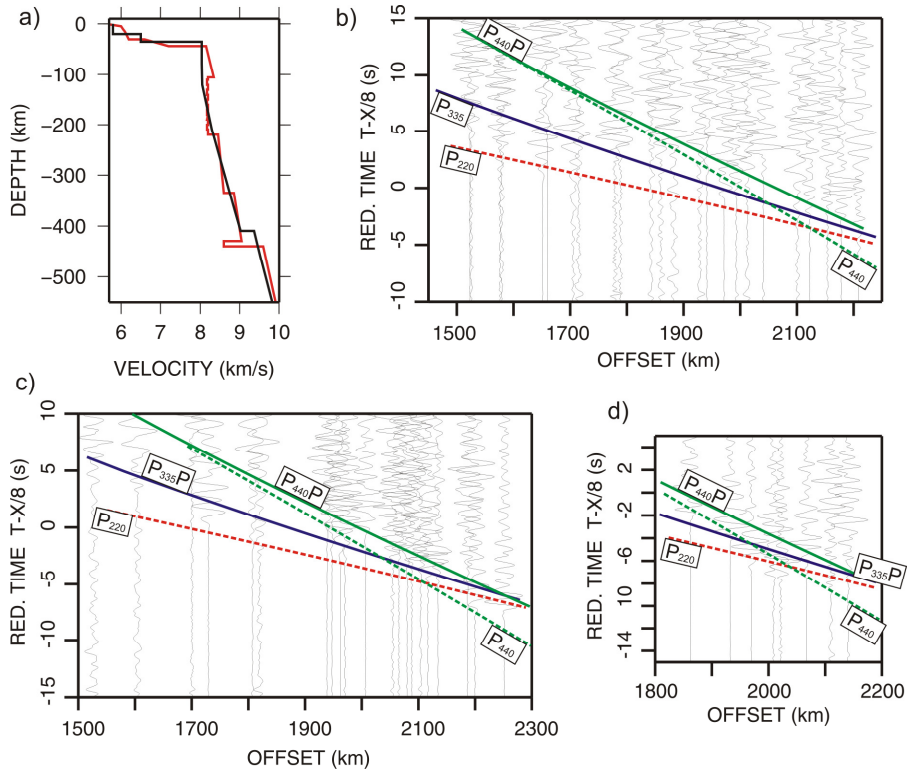

Figure 4. (a) The new MP1-SUW model (red line) compared with the AK 135 model (black line). **(b–d)** Seismic sections with traveltimes calculated for the MP1-SUW model for three focal depth ranges **(b)** 0–20 km, **(c)** 20–50 km, **(d)** > 50 km.

SED
6, 559–598, 2014

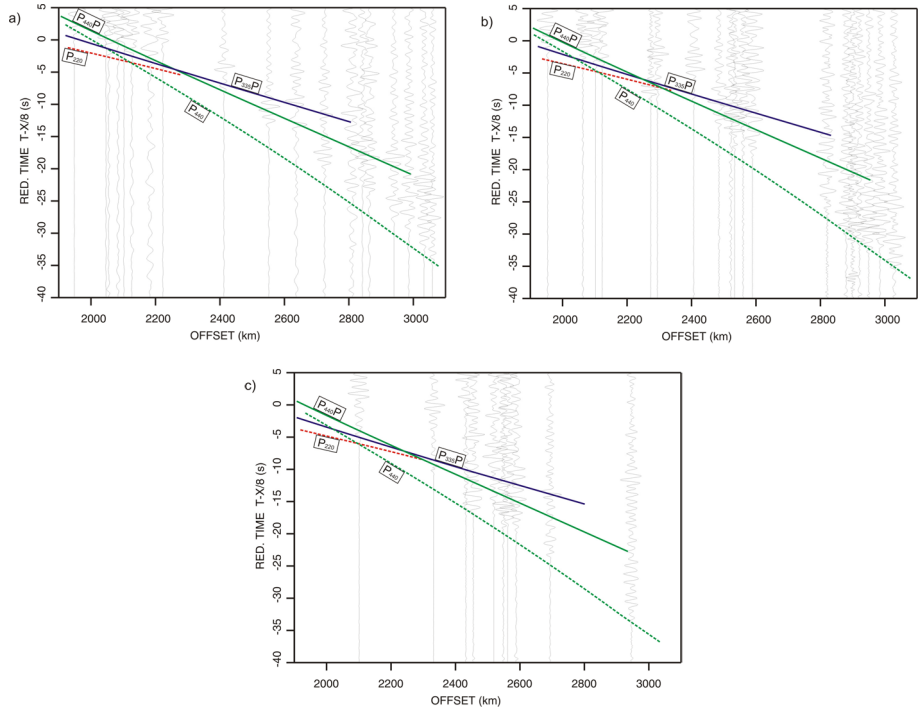

Figure 5. Seismic sections based on the data from the CR group with traveltimes calculated for the MP1-SUW model for three focal depth ranges **(a)** 0–20 km depth, **(b)** 20–50 km depth, **(c)** > 50 km.

SED
6, 559–598, 2014

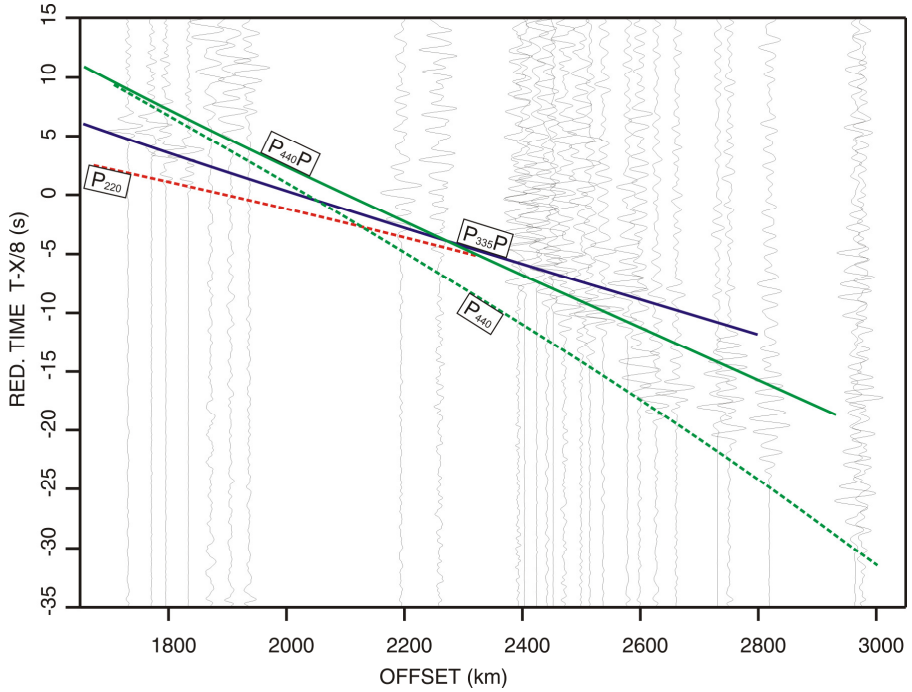

Figure 6. Seismic section based on data from the WMSR region with traveltimes calculated for the MP1-SUW model.

SED
6, 559–598, 2014

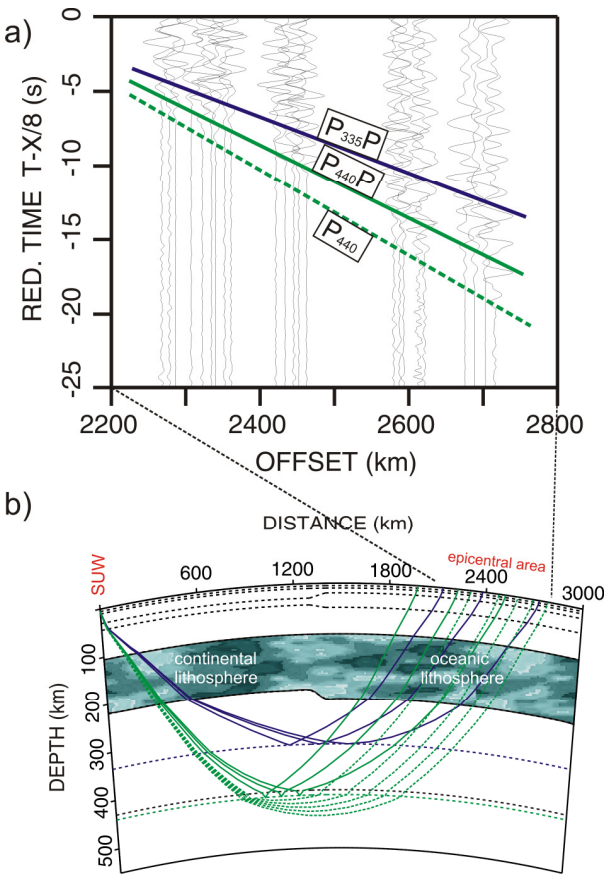

Figure 7. (a) Seismic section for the data from the JMR region with traveltimes calculated in the 2-D model shown in **(b)**. **(b)** 2-D ray-tracing model and the ray paths refracted and reflected at 335 km and 440 km discontinuities.

SED
6, 559–598, 2014

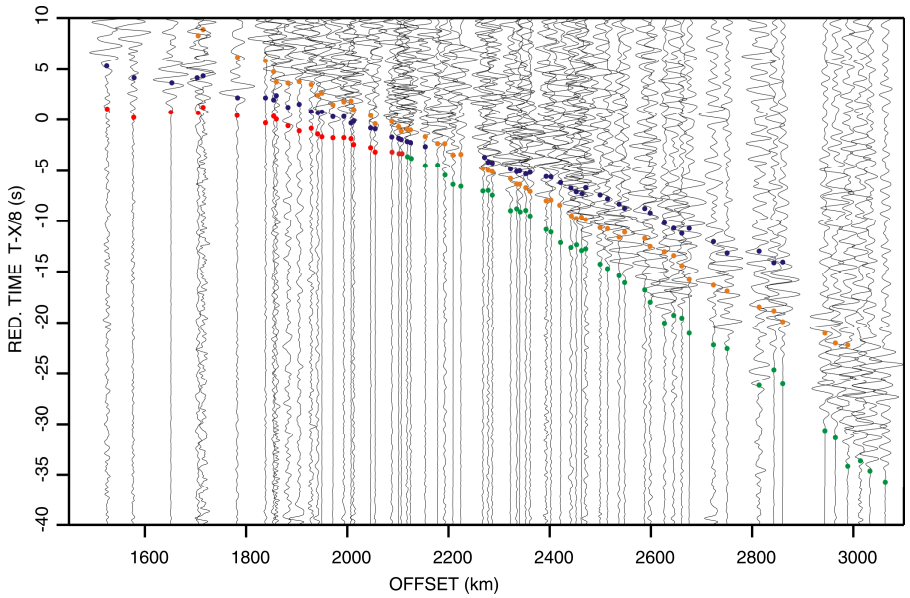

Figure 8. All analysed seismograms recorded at SUW station with the focal depth corrections applied. Red dots represents P_{200}, green – P_{440}, blue – $P_{335}P$, orange – $P_{440}P$ phases.

SED
6, 559–598, 2014

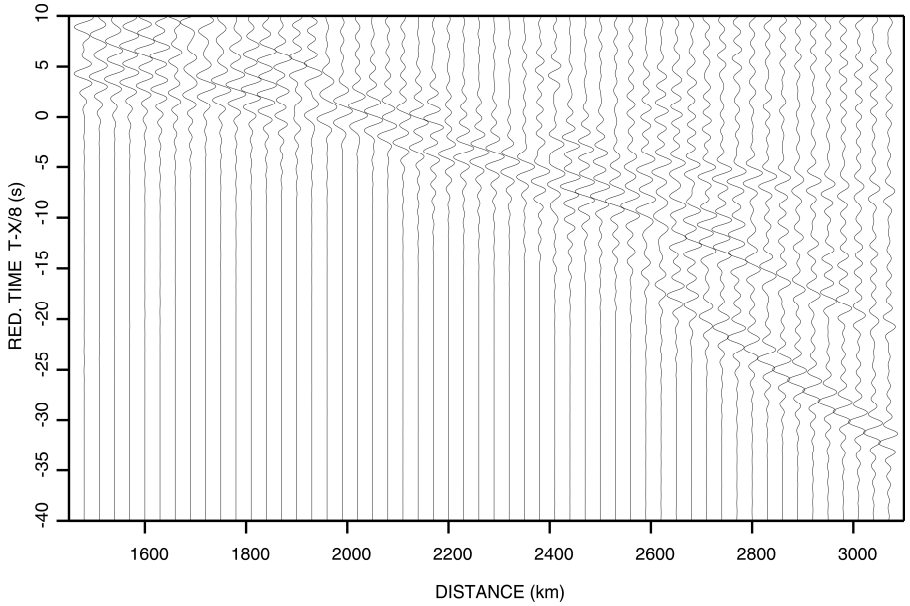

Figure 9. Synthetic seismograms section calculated for the MP1-SUW model using reflectivity method (0.1–2.0 Hz). Compare with data in Fig. 8.

SED
6, 559–598, 2014

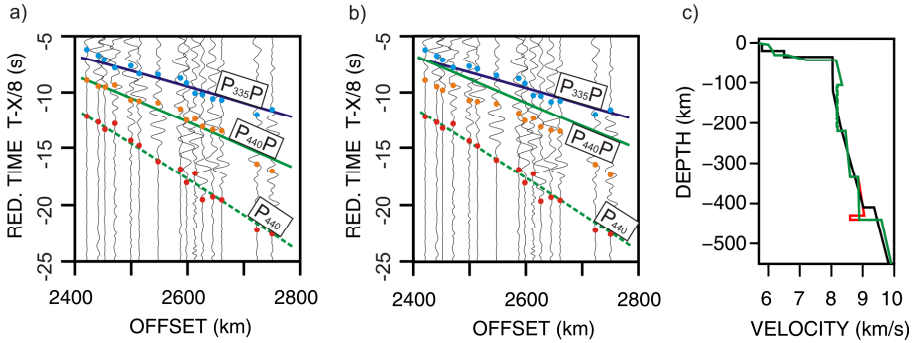

Figure 10. (a) Part of the seismic section with the MP1-SUW model traveltimes overlayed. Red dots represents P_{440}, orange – $P_{440}P$, blue – $P_{335}P$. **(b)** Part of the seismic section with the traveltimes calculated for the model without the LVZ atop the 440 km discontinuity. **(c)** Comparison of 1-D seismic velocity models. Red line corresponds to the MP1-SUW model and green line to the same model without LVZ atop 440 km discontinuity. Black line corresponds to the AK135 model.

SED
6, 559–598, 2014

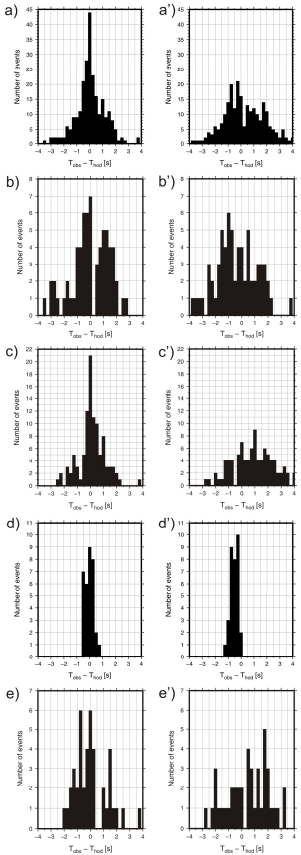

Figure 11. Histograms of the residuals between the observed traveltimes and the traveltimes calculated for the MP1-SUW model (left column) and between the observed traveltimes and the traveltimes calculated for the AK135 model (right column) for the following data: **(a) (a')** all events, **(b) (b')** events from the CR, **(c) (c')** events from the GTR, **(d) (d')** events from the JMR, **(e) (e')** events from the WMSR.

SED
6, 559–598, 2014

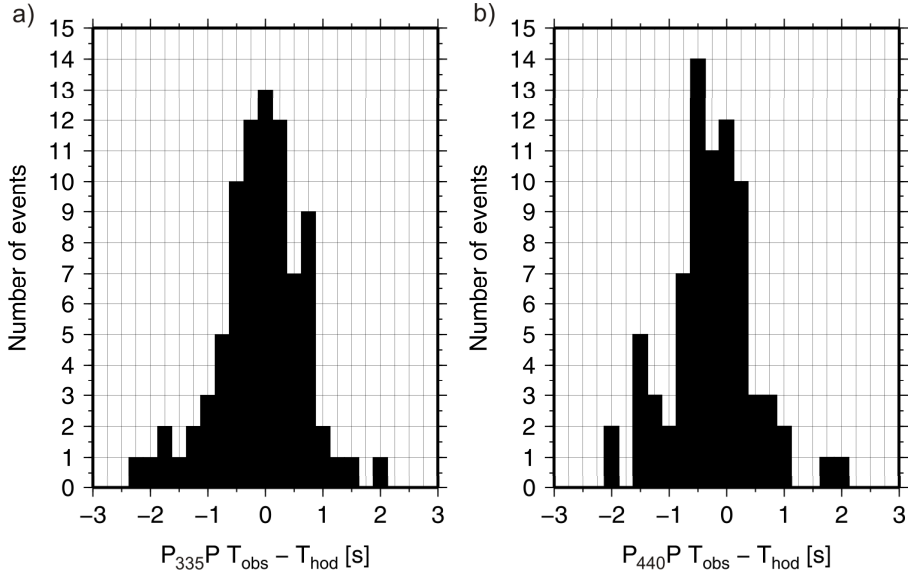

Figure 12. Histograms of the traveltime residuals between the reflected phases $P_{335}P$ (left column), the $P_{440}P$ ones (right column) and the calculated traveltimes for the MP1-SUW model.

SED
6, 559–598, 2014